Image Reconstruction by Phase Retrieval with Transverse Translation Diversity

Manuel Guizar-Sicairos and James R. Fienup

The Institute of Optics, University of Rochester, Rochester, New York, 14627, USA

ABSTRACT

Measuring a series of far-field intensity patterns from an object, taken after a transverse translation of the object with respect to a known illumination pattern, has been shown to make the problem of image reconstruction by phase retrieval much more robust. However, previously reported reconstruction algorithms [Phys. Rev. Lett. **93**, 023903 (2004)] rely on an accurate knowledge of the translations and illumination pattern for a successful reconstruction. We developed a nonlinear optimization algorithm that allows optimization over the translations and illumination pattern, dramatically improving the reconstructions if the system parameters are inaccurately known [Opt. Express **16,** 7264 (2008)]. In this paper we compare reconstructions obtained with these algorithms under realistic experimental scenarios.

Keywords: Phase retrieval, image reconstruction techniques, inverse scattering, coherent x-ray imaging

1. INTRODUCTION

The resolution of a diffraction-limited imaging system (in the absence of aberrations) is limited by the illumination wavelength and the location and diameter of the entrance pupil of the focusing optics. Because of the small wavelength and high penetration depth, x-rays promise imaging with very high resolution with the additional advantage of imaging through relatively thick structures. However, current manufacturing capabilities limit the performance of focusing optics in the x-ray regime, in terms of both the maximum numerical aperture and aberrations.

Image reconstruction by phase retrieval, a technique originally developed and demonstrated for optical wavelengths[1–4] was recognized as an alternative to conventional imaging for the x-ray regime.[5–8] For phase retrieval, the sample needs to be illuminated with a sufficiently coherent source and the intensity of the diffraction pattern is used to computationally retrieve the associated phase of the diffracted beam, thus yielding a diffraction-limited image. This is typically achieved by using a support constraint, a set of points outside of which the object is known to be zero and, when applicable, a nonnegativity constraint.[1–4,9,10]

There are techniques that can yield reconstruction with a direct computation by including in the plane of the sample a suitable reference,[11–15] but they have more stringent sampling requirement than phase retrieval and the resolution of the reconstruction is typically limited by the manufacturing capabilities for the reference feature.

Adding diversity to phase retrieval measurements has been proven to make the computational problem more robust to noise, inherent ambiguities and algorithm stagnation. By imparting a known modification to the setup and measuring the resulting diffraction patterns, the algorithms receive additional information that allows for superior reconstructions. For optical metrology, the detector is typically moved to different positions along the optical axis, thus obtaining a set of intensity measurements through focus. These measurements are then jointly used to retrieve the phase distribution associated to the measured intensities.[16,17] For x-ray imaging, however, the small object and large detector pixel pitch typically restrict the measurements to be taken in the far-field regime. In the far field, moving the detector in the direction of propagation results in a transverse magnification of the intensity pattern and does not provide suitable diversity.

A form of diversity that is practical for the x-ray imaging problem was first proposed by Faulkner and Rodenburg, along with a robust reconstruction algorithm: the ptychographical iterative engine (PIE).[18,19] In

Contact information: mguizar@optics.rochester.edu, fienup@optics.rochester.edu

Image Reconstruction from Incomplete Data V, edited by Philip J. Bones, Michael A. Fiddy, Rick P. Millane,
Proc. of SPIE Vol. 7076, 70760A, (2008) · 0277-786X/08/$18 · doi: 10.1117/12.792622

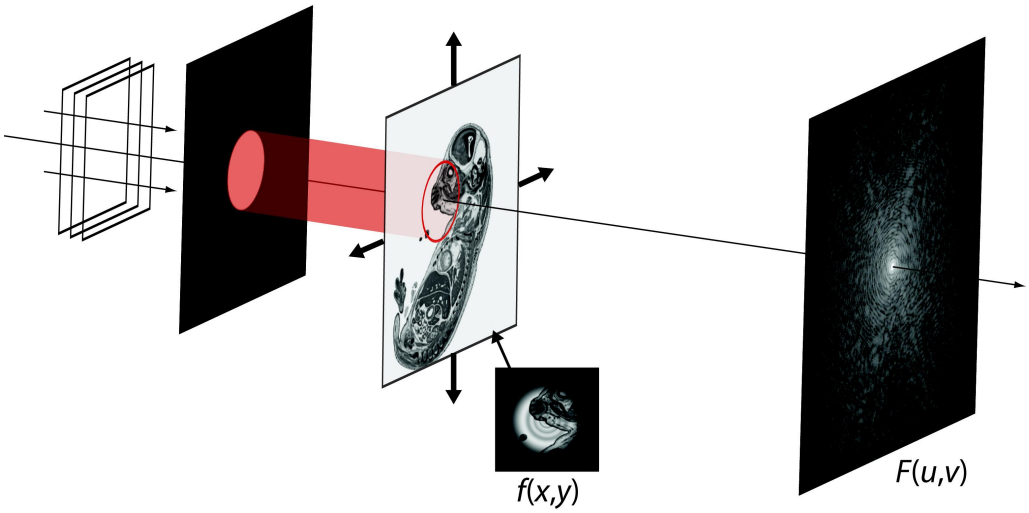

Figure 1. Example experimental setup for phase retrieval with transverse translation diversity. A plane wave is incident on an aperture. The field transmitted by the aperture propagates to the plane of the moveable object, thus generating the illumination pattern $p(x, y)$. The field transmitted by the object is then given by the product of the illumination pattern and the object transmissivity, $f_n(x, y) = o(x - x_n, y - y_n)p(x, y)$. A detector array is used to measure the far-field intensity pattern $I_n(u, v) = |F_n(u, v)|^2$.

this approach, phase retrieval with transverse translation diversity, the object is translated relative to a known illumination pattern, that can be either the diffracted field from an aperture, a focused field or an aperture itself, as illustrated in Fig. 1. The far-field intensity pattern is measured for each position of the moveable object (or equivalently the illumination pattern may be moved). These intensity measurements are then used, along with the *a priori* knowledge of the illumination pattern and the translations, to reconstruct the complex-valued transmissivity of the object.

The PIE relies on an accurate knowledge of the system parameters (the illumination pattern and the object translations) and the reconstruction is found to be affected by artifacts and errors if these parameters are inaccurately known. In this paper we describe a nonlinear optimization algorithm to solve the problem of phase retrieval with transverse translation diversity.[20] Through analytical expressions for the gradient of a squared-error metric with respect to the object, illumination and translations, this approach allows the recovery of the object while refining the initial estimate for the system parameters. We show that the nonlinear optimization approach yields superior reconstructions with reduced errors and artifacts when the system parameters are inaccurately known. Furthermore, because the nonlinear optimization approach uses all of the intensity measurements simultaneously (rather than sequentially as the PIE does), the reconstruction also exhibits reduced noise artifacts.

2. PHASE RETRIEVAL WITH A MOVEABLE OBJECT

Provided that the sample is thin, we can approximate the wave transmitted by the object by

$$f_n(x, y) = o(x - x_n, y - y_n)p(x, y), \tag{1}$$

where $p(x, y)$ is the known illumination pattern and $o(x - x_n, y - y_n)$ is the unknown object transmissivity, centered at (x_n, y_n). The phase retrieval problem with transverse translation diversity consists of measuring the diffracted intensity pattern for each position of the object and using these measurements to reconstruct $o(x, y)$.

Because for x-rays the detector pixel pitch (the separation between pixel centers) can be several times larger than the object, the measurement is typically taken in the far field. Within the paraxial approximation, the field at the plane of the detector is well approximated by the Fourier transform (FT) of the field at the plane of the object. The measured intensity pattern is then given by

$$I_n(u, v) = |F_n(u, v)|^2 , \tag{2}$$

where we have dropped unimportant multiplicative scaling factors. We approximate the FT with the discrete FT (DFT),

$$F_n(u,v) = |F_n(u,v)| \exp\left[i\theta_n(u,v)\right] = \mathrm{DFT}\left\{f_n(x,y)\right\} = \frac{1}{\sqrt{MN}} \sum_{x,y} f_n(x,y) \exp\left[-i2\pi\left(\frac{ux}{M} + \frac{vy}{N}\right)\right]. \quad (3)$$

The PIE is an iterative transform reconstruction approach, that updates the object estimate, $\hat{o}(x,y)$, by sequentially using the different intensity patterns.[19] This algorithm can be shown to be related to a steepest descent search.[20] For brevity we omit the description of the PIE which can be found in Ref. 19, the reader is also referred to Ref. 20 for a description of the PIE in the notation used in this paper.

For the nonlinear optimization approach we seek to minimize the squared-error metric

$$\varepsilon = \sum_{n=1}^{q} \sum_{u,v} W_n(u,v) \left\{ \left[|\hat{F}_n(u,v)|^2 + \delta \right]^{\gamma} - \left[I_n(u,v) + \delta \right]^{\gamma} \right\}^2, \quad (4)$$

where

$$\hat{F}_n = \mathrm{DFT}\left\{\hat{f}_n(x,y)\right\} = \mathrm{DFT}\left\{\hat{o}(x-\hat{x}_n, y-\hat{y}_n)\hat{p}(x,y)\right\}, \quad (5)$$

γ is a real-valued constant, δ is a small constant that prevents problems in the gradient computation where I_n is close to zero, and $W_n(u,v)$ is a weighting function that can be used to emphasize regions with high SNR or set to zero for regions with poor SNR or where no signal was measured. The weighting function can be set to zero for dead or saturated pixels or in the region affected by a beam stop.

The number of parameters over which we need to optimize to solve for the object, $\hat{o}(x,y)$, is equal to the number of pixels in the object, thus making a finite-difference gradient computation prohibitively time consuming. Efficient implementation of the nonlinear optimization algorithm relies on having an analytical expression for the gradient of the error metric with respect to the object parameters. This gradient is given by,

$$\frac{\partial \varepsilon}{\partial \hat{o}_{\mathrm{R}}(x,y)} + i\frac{\partial \varepsilon}{\partial \hat{o}_{\mathrm{I}}(x,y)} = 4\sum_{n=1}^{q} \hat{p}^*(x+\hat{x}_n, y+\hat{y}_n)\mathrm{IDFT}\Bigg\{ W_n \left[\left(|\hat{F}_n|^2 + \delta \right)^{\gamma} - \left(I_n + \delta \right)^{\gamma} \right] \times \gamma \left(|\hat{F}_n|^2 + \delta \right)^{\gamma-1} \hat{F}_n \exp\left[i2\pi \left(\frac{u\hat{x}_n}{M} + \frac{v\hat{y}_n}{N} \right) \right] \Bigg\}, \quad (6)$$

where $\mathrm{IDFT}\{\cdot\}$ is the inverse discrete Fourier transform.

A crucial advantage of the nonlinear optimization algorithm over the PIE is the ability of the former to refine the initial estimate of the illumination pattern and the translations. The gradient of ε with respect to the illumination pattern, $\hat{p}(x,y)$, is given by

$$\frac{\partial \varepsilon}{\partial \hat{p}_{\mathrm{R}}(x,y)} + i\frac{\partial \varepsilon}{\partial \hat{p}_{\mathrm{I}}(x,y)} = 4\sum_{n=1}^{q} \hat{o}^*(x-\hat{x}_n, y-\hat{y}_n)\mathrm{IDFT}\Bigg\{ W_n \left[\left(|\hat{F}_n|^2 + \delta \right)^{\gamma} - \left(I_n + \delta \right)^{\gamma} \right] \gamma \left(|\hat{F}_n|^2 + \delta \right)^{\gamma-1} \hat{F}_n \Bigg\}, \quad (7)$$

and the gradient with respect to the translations, $(\hat{x}_n, \hat{y}_n)$, is given by

$$\frac{\partial \varepsilon}{\partial \hat{x}_n} = \frac{8\pi}{M} \sum_{u,v} W_n \left[\left(|\hat{F}_n|^2 + \delta \right)^{\gamma} - \left(I_n + \delta \right)^{\gamma} \right] \gamma \left(|\hat{F}_n|^2 + \delta \right)^{\gamma-1} \times \mathrm{Im}\left[\hat{F}_n^* \ \mathrm{DFT}\left(\hat{p}(x,y) \ \mathrm{IDFT}\left\{ u'\hat{O}(u',v') \exp\left[-i2\pi \left(\frac{u'\hat{x}_n}{M} + \frac{v'\hat{y}_n}{N} \right) \right] \right\} \right) \right] \quad (8a)$$

$$\frac{\partial \varepsilon}{\partial \hat{y}_n} = \frac{8\pi}{N} \sum_{u,v} W_n \left[\left(|\hat{F}_n|^2 + \delta \right)^{\gamma} - \left(I_n + \delta \right)^{\gamma} \right] \gamma \left(|\hat{F}_n|^2 + \delta \right)^{\gamma-1} \times \mathrm{Im}\left[\hat{F}_n^* \ \mathrm{DFT}\left(\hat{p}(x,y) \ \mathrm{IDFT}\left\{ v'\hat{O}(u',v') \exp\left[-i2\pi \left(\frac{u'\hat{x}_n}{M} + \frac{v'\hat{y}_n}{N} \right) \right] \right\} \right) \right]. \quad (8b)$$

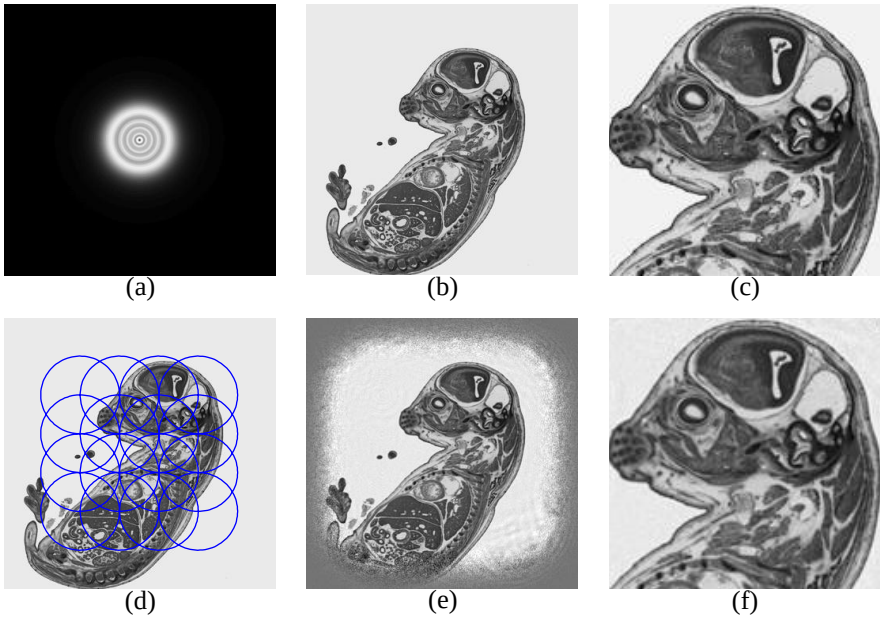

Figure 2. Amplitude of (a) the illumination pattern at the plane of the object and (b) the object transmissivity. For better visualization we show in (c) a 160×160 pixel inset of the object. (d) Location and approximate support of the illumination pattern for the different object translations. (e) Reconstruction after 50 iterations of the PIE. (f) 160×160 inset of (e). 340×340 insets of the full 512×512 arrays are shown in (a), (b), (d) and (e).

3. NUMERICAL SIMULATIONS

In this section we show numerical simulations of data acquisition and compare reconstructions using the PIE and our nonlinear optimization algorithm.

Figure 2(b) shows a 340×340 inset of the 512×512 image of a rodent embryo[21] that was used as the unknown object amplitude distribution. The illumination pattern at the plane of the object, $p(x, y)$, is shown in Fig. 2(a). This pattern was generated from the free-space propagation of a field transmitted by a circular aperture with a radius of 1 micron (50 pixels). The circular aperture was assumed to be illuminated by a plane wave with a wavelength of 0.1 nm and to be located 1 mm before the object.

The measured diffraction patterns were obtained by translating the object by 50 pixels across a 4×4 Cartesian grid. Figure 2(d) shows the location and approximate extent of the illumination pattern for different object translations. Because $p(x, y)$ is the diffraction pattern from an aperture, it has sidelobes that extend indefinitely. The product of the illumination pattern and the translated object is then taken to obtain the field at the plane of the object, $f_n(x, y)$. We then compute the DFT of the object-space field and take the squared-modulus to arrive at the far-field intensity measurements $I_n(u, v)$. The diffraction patterns were normalized to have a maximum of 10^5 photons on the brightest pixel and Poisson distributed noise was applied to them. Figure 2(e) shows the amplitude of the object reconstruction after 50 iterations of the PIE. For this experiment, the initial estimate of the object was a uniform real-valued distribution and we assumed a perfect knowledge of the illumination pattern and the translations. For easier visualization, smaller insets of the object and the reconstruction are shown in Figs. 2(c) and 2(f), respectively. We obtained a very good estimate of the object transmissivity within the support sampled by the illumination pattern.

To illustrate the effect of inaccurate characterization of the system parameters, we performed an additional numerical simulation. Here, the magnitude of the object translations were perturbed by zero-mean additive Gaussian noise, the root-mean-squared (RMS) shift error was 35.2 nm (1.762 pixels). The illumination pattern, $p(x, y)$, used to simulate the far-field diffraction patterns, was not generated through diffraction from a perfectly

circular aperture, but from an aperture whose radius had a weak dependence on the azimuthal angle. The imperfect circular aperture and the resulting illumination pattern are shown in Figs. 3(a) and 3(d) respectively. We wish to emphasize that phase retrieval with transverse translation diversity works with any illumination pattern, whether diffracted by a circular aperture or any other arbitrary shape; it is the inaccurate characterization of this aperture that introduces artifacts in the reconstruction.

The initial estimate of $p(x, y)$ for the reconstruction algorithm was given by the diffraction pattern of a perfect circular aperture, and we assumed that the distance from the aperture to the object (1 mm) is accurately known. Notice that the deviation from a perfect circle of the aperture shown in Fig. 3(a) is subtle and that the resulting diffraction pattern [Fig. 3(d)] is visually indistinguishable from that generated from the perfectly circular aperture [Fig. 2(a)]. The difference between the aperture in Fig. 3(a) and that of a perfect circle is shown in Fig. 3(g), where gray is assigned to zero difference, dark pixels and light pixels correspond to regions where the perfect circle is larger or smaller than the aperture, respectively. The maximum difference in this case was less than 30% of the maximum aperture transmissivity. In order to reduce discretization artifacts we introduced a slight tapering across the edges of the apertures. The error in the transmissivity is less than unity because the error lies within these tapered regions. The normalized (RMS) error of this aperture with respect to the perfect circle used as input to the reconstruction algorithms is $(\sum |h - \hat{h}|^2 / \sum |h|^2)^{1/2} = 0.03$.

Figures 3(b) and 3(c) show the reconstruction result after 500 iterations of the PIE. Upon comparison with the original object, shown in Figs. 2(b) and 2(c), we see that even though the error in the system parameters is relatively small, the reconstruction suffers from artifacts. Although the object is recognizable, the very finest details and low-contrast features become hard to discern. The PIE stagnates after about 100 iterations and does not make further progress in the reconstruction.

The reconstruction after 500 iterations of the nonlinear optimization algorithm, for $\gamma = 0.5$, is shown in Figs. 3(e) and 3(f). Notice that this reconstruction is greatly improved when compared to the result of the PIE, shown in Figs. 3(b) and 3(c). For the reconstruction in Fig. 3(e), the gradients in Eqs. (6)-(8) were used along with a conjugate-gradient nonlinear optimization routine. We define an iteration as every time the gradient needs to be computed. Best results were obtained by optimizing over only the object for the first few iterations. The first 10 iterations were done with the PIE, to take advantage of its speed (for this case an iteration of the PIE algorithm is about 4× faster); then we performed 15 iterations with the nonlinear optimization algorithm but optimizing only over the object. In doing this we obtained an intermediate object estimate that minimizes the error metric, ε, given by Eq. (4). After this we performed further iterations optimizing jointly over the object, illumination and translations.

We evaluate the error of the reconstructions with respect to the ideal object through the normalized, translation-invariant field RMS error (NRMSE), E, given by

$$E^2 = \frac{1}{q} \sum_{n=1}^{q} \left[\min_{\rho_n, x', y'} \frac{\sum_{x,y} \left| \rho_n \hat{f}_n(x - x', y - y') - f_n(x, y) \right|^2}{\sum_{x,y} |f_n(x, y)|^2} \right]. \tag{9}$$

This error metric is a measure of the difference between the ideal and reconstructed complex-valued fields for the different object positions. Computation of E, requires knowledge of the true solution to the phase retrieval problem, and it is then only available for numerical simulations. Because for each position of the object we only measure the intensity of its Fourier transform, we cannot detect a global phase constant or the absolute position of the object; it is then important to evaluate the error in the reconstructions through a metric that is invariant to these operations. For this purpose E is minimized with respect to a complex-valued multiplicative constant and a transverse translation of each field. Equation (9) can be evaluated by registering f_n and $\hat{f}_n$ within a small fraction of a pixel by cross-correlation.[22,23] For the results shown in this paper we registered the fields to within 1/25 of a pixel by means of an efficient algorithm for image registration.[23]

Figure 3(h) shows the reconstruction error, E, versus iteration number for the PIE and the nonlinear optimization algorithm. Notice that the reconstruction with the nonlinear optimization algorithm has a significantly smaller error. The RMS shift error, Δr, is shown in Fig. 3(i) versus iteration number. Because only the relative displacements of the object are important for the reconstruction and not the absolute position of the object,[19,20]

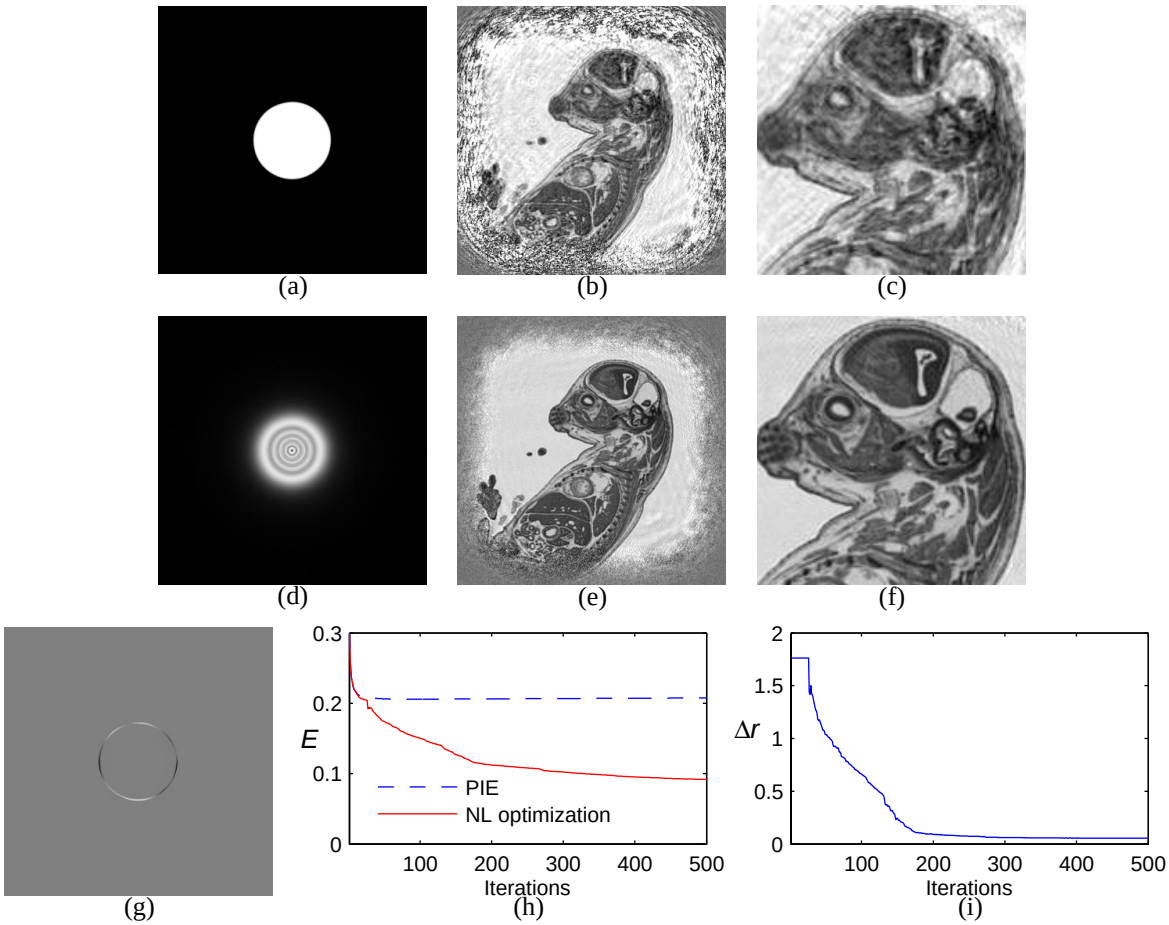

Figure 3. (a) Unit transmissivity aperture that generates (d) the illumination pattern at the object plane, $p(x, y)$. The aperture shape slightly deviates from a perfect circle. Reconstruction after 500 iterations of (b) the PIE and (e) the nonlinear optimization algorithm. 160×160 insets of (b) and (e) are shown in (c) and (f), respectively. (g) Difference between the aperture and the perfect circle used for estimating $\hat{p}(x, y)$ for reconstruction. (h) NRMSE of the reconstructions vs. iteration number. (i) Shift error, Δr, in units of pixels vs. iteration number. Difference in (e) is shown in the range $(-0.3, 0.3)$, these limits correspond to black and white, respectively. 340×340 insets of the 512×512 arrays are shown in (a), (b), (d), (e) and (g).

we evaluated a global-shift-invariant version of the RMS error.[20] For the first 25 iterations Δr remains constant because we optimized only over the object; for subsequent iterations the shift error progressively decreases.

To further test the performance of the nonlinear optimization algorithm, we performed an additional numerical simulation. In this case, the aperture that generates $p(x, y)$ was an accurately known circular aperture. However, we assumed an error in the measurement of the distance from the aperture to the object. The illumination pattern at the plane of the object, shown in Fig. 4(a), was obtained by propagating the field transmitted by a circular aperture with a radius of 1 μm (50 pixels) by 1.05 mm. The estimate of the illumination pattern used for reconstruction, $\hat{p}(x, y)$, was obtained by propagating the field transmitted by the same aperture but for a distance of 1 mm, as shown in Fig. 2(a). We then introduced an error of 50 μm in the characterization of the distance from the aperture to the object. We also added a small error, $\Delta r = 1$ pixel, in the estimate of the translation parameters, (x_n, y_n).

We normalized the far-field intensity patterns to have a maximum of about 10^5 photons on the brightest pixel and applied Poisson distributed noise. The reconstruction after 1500 iterations of the PIE and the nonlinear optimization algorithm are shown in Figs. 4(b) and 4(e), respectively. The initial estimate of the object for

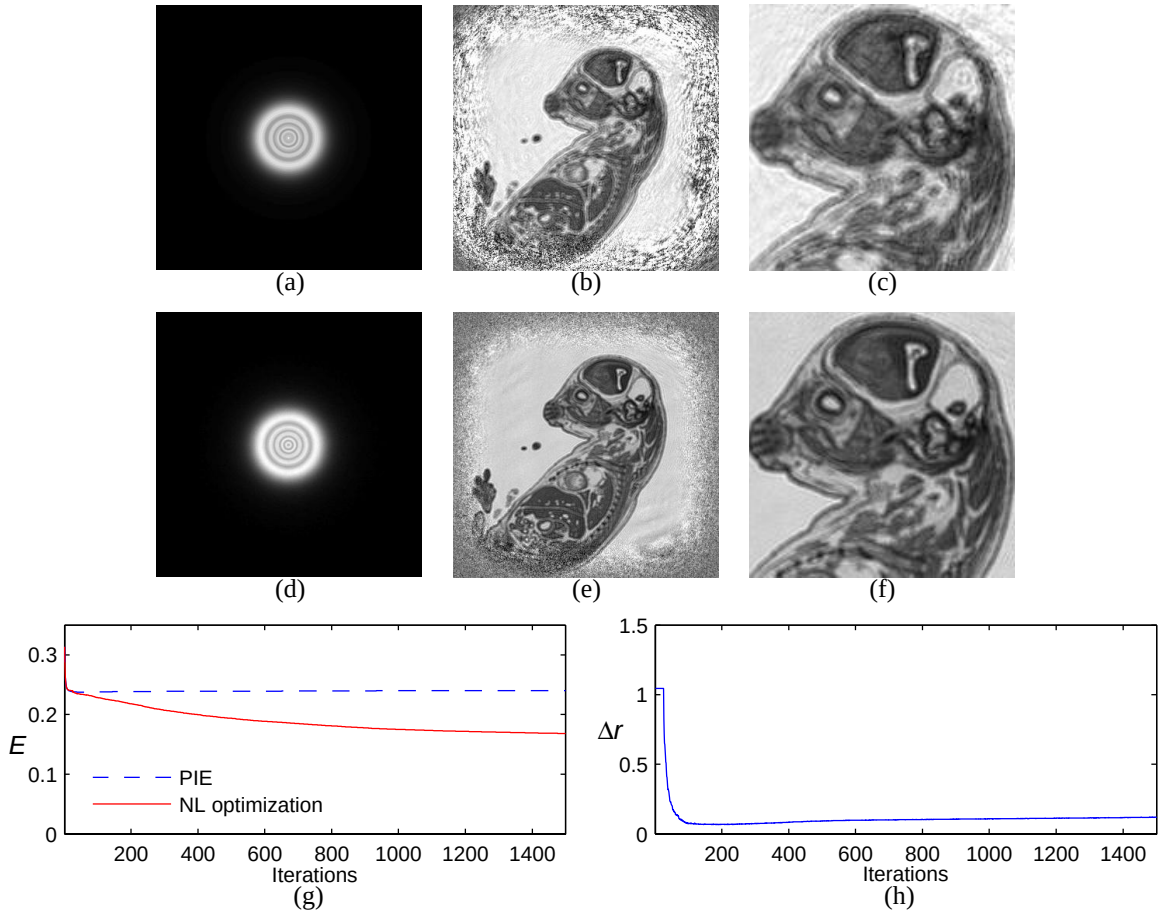

Figure 4. (a) Illumination pattern, $p(x, y)$, obtained after a 1.05 mm propagation of the field transmitted by a circular aperture. The initial estimate of the illumination pattern, $\hat{p}(x, y)$, used for reconstruction is obtained after a 1 mm propagation and is shown in Fig. 2(a). Reconstruction after 1500 iterations of (b) the PIE and (e) the nonlinear optimization algorithm. 160×160 insets of (b) and (e) are shown in (c) and (f) respectively. (d) Final estimate of the illumination pattern after joint optimization of the object and system parameters. (g) NRMSE of the reconstructions vs. iteration number. (h) Shift error, Δr, in units of pixels vs. iteration number. 340×340 insets of the full 512×512 arrays are shown in (a), (b), (d) and (e).

both reconstructions was a real-valued uniform distribution. Again we notice that the PIE stagnated after a few iterations and, although it yields good results, the residual artifacts blur the very fine details of the object and reduce feature contrast. For the reconstruction with the nonlinear optimization algorithm we performed 10 iterations of the PIE, followed by 15 iterations where we optimized only over the object. Further iterations were performed jointly optimizing over the object, illumination and translations. Notice that the final reconstruction, shown in Figs. 4(e) and 4(f), has significantly reduced artifacts as compared with the PIE reconstruction, and that the fine details are easier to discern. The NRMSE and shift error are shown versus iteration number in Figs. 4(g) and 4(h), respectively.

Notice that this reconstruction proved to be a particularly difficult one. In comparison with the previous example, this reconstruction required a significantly increased number of iterations (convergence was slower). For this reconstruction, most of the error in the system parameters resides in the characterization of $p(x, y)$. Because we did not assume any prior knowledge about the nature of the system parameter error, we needed to optimize the $p(x, y)$ on a point-by-point basis. This significantly increased the number of parameters to optimize and made the reconstruction in general more difficult.

The final estimate of the illumination pattern is shown in Fig. 4(d); notice that it has still not quite arrived to the true illumination pattern shown in Fig. 4(a) and more iterations are needed to refine this estimate. Despite this disagreement, the nonlinear optimization has brought the illumination pattern estimate to a point where the artifacts in the reconstruction are greatly diminished, as shown in Figs. 4(e) and 4(f).

In Ref. 20 we demonstrated the ability of the nonlinear optimization algorithm to successfully refine the estimate of $\hat{p}(x, y)$ in a point-by-point basis, with reasonable convergence. Here showed that for some cases, especially as the error in our estimate of the aperture increases, the refinement of the illumination pattern may be more difficult, but still the object estimate exhibits a superior quality than the one obtained by optimizing only over the object.

An improved convergence for the nonlinear optimization algorithm (reduction in the required number of iterations) could be achieved if in the reconstruction we could explicitly make use of the fact that the error originates from an inaccurate measurement of the distance from the aperture to the object. In that case we would be able to optimize the illumination pattern with respect to only one parameter: the propagation distance. Alternatively, we have found that increasing the number of diffraction patterns (having additional translations for the object) can also improve the convergence of the reconstruction.

4. CONCLUSIONS

The push for higher resolution imaging in the x-ray regime is driven by the ultimate tradeoff between relaxing experimental requirements and increasing computational postprocessing. For coherent lensless imaging, the focusing optics are replaced by algorithms that computationally retrieve the phase associated with the measured diffraction pattern intensity and reconstruct a diffraction-limited image of the object.

Transverse translation diversity is a form of diversity for phase retrieval that makes reconstructions fast, robust and reliable. However, it previously relied on having accurate characterization of the illumination pattern and the object translations. We have observed that good reconstructions can be obtained, even in the presence of noise and small errors in the characterization of the experimental parameters. However, errors in the illumination pattern and translations yield reconstructions that suffer from artifacts that blur or obscure the fine details of the reconstruction. We have shown that significant artifacts are introduced on the reconstruction, even for shift errors that are on the order of the final image resolution. For imaging with a resolution of a few nanometers, having translation errors smaller than the expected resolution places a substantial burden on the experiment stability and the quality and calibration of the translating stages.

There are multiple potential sources of error for the system parameters. For example, even if we know the physical dimensions of the aperture very precisely, an inaccurate measurement of the distance from the object to the detector can yield an undesired scaling of the size of the aperture in the computational window. This scaling error can introduce very severe artifacts on the reconstruction.[20] The illumination pattern may also differ from our estimate if the aperture is not illuminated by a plane wave but rather by a beam that is not accurately characterized. The beam incident on the aperture may present unknown variations of amplitude and phase that will distort the illumination pattern and negatively affect the reconstructions.

Our new nonlinear optimization algorithm is a further step in the drive of relaxing the experimental requirements by placing an additional burden on the algorithms used for reconstruction. Our approach allows reconstruction of the unknown object while jointly refining the initial estimates of the translation and the illumination pattern. Use of the nonlinear optimization algorithm in this case relaxes the experimental requirements and achieves superior reconstructions.

REFERENCES

[1] J. R. Fienup, "Phase retrieval algorithms: a comparison," Appl. Opt. **21,** 2758–2769 (1982).

[2] J. R. Fienup, "Reconstruction of a complex-valued object from the modulus of its Fourier transform using a support constraint," J. Opt. Soc. Am. A **4,** 118–123 (1987).

[3] P. S. Idell, J. R. Fienup and R. S. Goodman, "Image synthesis from nonimaged laser-speckle patterns," Opt. Lett. **12,** 858–860 (1987).

[4] J. N. Cederquist, J. R. Fienup, J. C. Marron and R. G. Paxman, "Phase retrieval from experimental far-field speckle data," Opt. Lett. **13,** 619–621 (1988).
[5] J. Miao, P. Charalambous, J. Kirz and D. Sayre, "Extending the methodology of X-ray crystallography to allow imaging of micrometre-sized non-crystalline specimens," Nature (London) **400,** 342–344 (1999).
[6] S. Marchesini, H. He, H. N. Chapman, S. P. Hau-Riege, A. Noy, M. R. Howells, U. Weierstall and J. C. H. Spence, "X-ray image reconstruction from a diffraction pattern alone," Phys. Rev. B **68,** 140101 (2003).
[7] H. N. Chapman *et al.*, "High-resolution *ab initio* three-dimensional x-ray diffraction microscopy," J. Opt. Soc. Am. A **23,** 1179–1200 (2006).
[8] J. Miao, T. Ishikawa, Q. Shen and T. Earnest, "Extending x-ray crystallography to allow the imaging of noncrystalline materials, cells and single protein complexes," Annu. Rev. Phys. Chem. **59,** 387–410 (2008).
[9] J. R. Fienup, "Lensless coherent imaging by phase retrieval with an illumination pattern constraint," Opt. Express **14,** 498–508 (2006).
[10] M. Guizar-Sicairos and J. R. Fienup, "Phase retrieval with Fourier-weighted projections," J. Opt. Soc. Am. A **25,** 701–709 (2008).
[11] E. N. Leith and J. Upatnieks, "Reconstructed wavefronts and communication theory," J. Opt. Soc. Am. **52,** 1123–1130 (1962).
[12] J. W. Goodman, *Introduction to Fourier Optics, 3rd Ed.* (Roberts & Company, Englewood, 2005).
[13] O. Hellwig, S. Eisebitt, W. Eberhardt, W. F. Schlotter, J. Lüning and J. Stöhr, "Magnetic imaging with soft x-ray spectroholography," J. Appl. Phys. **99**, 08H307 (2006).
[14] S. G. Podorov, K. M. Pavlov and D. M. Paganin, "A non-iterative reconstruction method for direct and unambiguous coherent diffractive imaging," Opt. Express **15**, 9954–9962 (2007).
[15] M. Guizar-Sicairos and J. R. Fienup, "Holography with extended reference by autocorrelation linear differential operation," Opt. Express **15**, 17592–17612 (2007).
[16] R. G. Paxman, T. J. Schulz and J. R. Fienup, "Joint estimation of object and aberrations by using phase diversity," J. Opt. Soc. Am. A **9,** 1072–1085 (1992).
[17] G. R. Brady and J. R. Fienup, "Nonlinear optimization algorithm for retrieving the full complex pupil function," Opt. Express **14,** 474–486 (2006).
[18] H. M. L. Faulkner and J. M. Rodenburg, "Movable aperture lensless transmission microscopy: a novel phase retrieval algorithm," Phys. Rev. Lett. **93,** 023903 (2004).
[19] J. M. Rodenburg and H. M. L. Faulkner, "A phase retrieval algorithm for shifting illumination," Appl. Phys. Lett. **85,** 4795–4797 (2004).
[20] M. Guizar-Sicairos and J. R. Fienup, "Phase retrieval with transverse translation diversity: a nonlinear optimization approach," Opt. Express **16,** 7264–7278 (2008).
[21] Image modified from an original courtesy of BrainMaps.org, by permission.
[22] J. R. Fienup, "Invariant error metrics for image reconstruction," Appl. Opt. **36,** 8352–8357 (1997).
[23] M. Guizar-Sicairos, S. T. Thurman and J. R. Fienup, "Efficient subpixel image registration algorithms," Opt. Lett. **33,** 156–158 (2008).